Polymer Degradation and Stability 230 (2024) 111047

Contents lists available at ScienceDirect

Polymer Degradation and Stability

journal homepage: www.journals.elsevier.com/polymer-degradation-and-stability

Phosphorus/boron-containing, flame-retardant polyurethane elastomers with great mechanical, shape-memory, and recycling performances

Tiantian Zhang [a], Siqi Huo [b,*], Guofeng Ye [a], Cheng Wang [a], Qi Zhang [a], Yijiao Xue [c], Pingan Song [d], Hao Wang [b], Zhitian Liu [a,*]

[a] Hubei Engineering Technology Research Center of Optoelectronic and New Energy Materials, School of Materials Science & Engineering, Wuhan Institute of Technology, Wuhan 430205, PR China
[b] Centre for Future Materials, School of Engineering, University of Southern Queensland, Springfield 4300, Australia
[c] Institute of Chemical Industry of Forest Products, Chinese Academy of Forestry (CAF), Nanjing 210042, PR China
[d] Centre for Future Materials, School of Agriculture and Environmental Science, University of Southern Queensland, Springfield 4300, Australia

ARTICLE INFO

Keywords:
Polyurethane elastomer
Flame retardancy
Mechanical properties
Recyclability
Shape memory

ABSTRACT

Based on sustainable development strategy and practical application requirement, it is crucial to develop high-strength, recyclable, and flame-retardant polyurethane (PU) elastomers. Hence, a flame-retardant, reprocessable, high-performance polyurethane elastomer (PU-DP 1–7) with dynamic boronic ester bonds and phosphorus-containing groups was well-designed and prepared. The chemical structure of PU-DP 1–7 was confirmed by Fourier transform infrared spectrometry (FTIR) and X-ray photoelectron spectroscopy (XPS). PU-DP 1–7 shows a transmittance of about 60 % at the wavelength of 900 nm, and phosphorus and boron elements are evenly distributed within its surface, confirming the formation of uniform cross-linking network. The inclusion of phosphorus-and boron-containing groups endows PU-DP 1–7 with a vertical combustion (UL-94) V-0 rating, indicative of desired flame retardancy. In addition, PU-DP 1–7 exhibits a tensile strength of 42.7 MPa and an elongation at break of 616.9 %, with high adhesion strengths towards various substrates due to abundant hydrogen bonds within its network. Furthermore, the dynamic borate ester bonds endow PU-DP 1–7 with superior physical recycling and shape-memory properties. After hot-pressing at 130 °C, the reformed PU-DP 1–7 film shows an 83.6 % recovery efficiency in terms of elongation at break. This work presents an integrated strategy to create flame-retardant, recyclable polyurethane elastomers with great mechanical and shape-memory performances by introducing phosphorus-containing segments and dynamic boronic ester bonds.

1. Introduction

Polyurethane elastomers are extensively used in aerospace [1,2], automotive industry [3,4], electronic skin [5], medical equipment [6,7], and wearable electronic devices [5,8,9] due to their high mechanical strength and elasticity. However, with the increasing plastic pollution, more and more attention has been paid to the development of recyclable and reprocessable polyurethane elastomers. Additionally, as traditional polymeric materials, the polyurethane elastomers are highly flammable and produce great deal of molten droplets upon ignited, restricting their applications. Compared with introducing flame retardant additives, covalently linking flame-retardant groups into the network of polyurethane elastomers can avoid the degradation of flame retardant performances in long-term application due to the migration problem [10].

Many works have confirmed that chemically introducing P-containing groups into polyurethane elastomers can effectively enhance flame retardancy. Zhao et al. [11] synthesized a waterborne polyurethane coating (SPU) using 1,4-butane diol (BDO) and [bis (2-hydroxyethyl)amino]-methyl- phosphonic acid dimethyl ester (BH), of which the limiting oxygen index (LOI) can be up to 28.2 % and the tensile strength can be obviously increased due to the introduction of BH. Song et al. [10] developed a P-containing PU, which showed a high LOI of 32.8 %, a UL-94 V-0 rating, and a high toughness of 460 MJ m^{-3}. Xue et al. [12] prepared a thermoplastic polyurethane (PU-RD) by using an abietic acid-based, phosphaphenanthrene-containing compound as a hard segment and polycaprolactone diol (PCL) as a soft segment, and physically cross-linked it with cellulose nanocrystals (CNC). The PU-RD/3.0CNC with 3.0 wt% of CNC exhibited a tensile strength of 9.1

* Corresponding authors.
E-mail addresses: sqhuo@hotmail.com, Siqi.Huo@unisq.edu.au (S. Huo), able.ztliu@wit.edu.cn (Z. Liu).

https://doi.org/10.1016/j.polymdegradstab.2024.111047
Received 6 August 2024; Received in revised form 9 October 2024; Accepted 18 October 2024
Available online 19 October 2024

MPa and an elongation at break of 560 %, with a UL-94 V-0 rating. Furthermore, PU-RD/5.0CNC with 5.0 wt% of CNC can be recycled in *N, N*-dimethylacetamide (DMAc). Wang et al. [13] developed a cyclotriphosphazene-containing polyurethane composite (FPCM-4) based on reversible furan/maleimide Diels–Alder (DA) reaction. FPCM-4 achieved a tensile strength of 19.8 MPa, an LOI value of 23.9 %, and a self-healing rate of 93.1 %. Therefore, these works have confirmed that the recyclable PU can be developed based on the reversible covalent/non-covalent bonds and covalently linking P-containing groups to polyurethane network can enhance flame retardancy. However, the reported PU elastomers usually suffered from poor mechanical properties. Hence, achieving the performance portfolio of superior mechanical, flame-retardant, and recycling properties is still a huge challenge [14-17].

To achieve the ideal flame-retardant effect, introducing synergistic flame-retardant elements, such as nitrogen, boron, and silicon, into P-containing flame-retardant systems has been proven to be an effective method [18-21]. Boron-based flame retardants mainly function in the condensed phase during combustion, which can form a glassy char on the matrix surface to suppress the heat release and the generation of molten droplets [22]. Thus, integrating boron and phosphorus into polyurethane network may effectively enhance the flame retardancy and anti-dripping performances of polyurethane elastomers. Moreover, forming abundant boronic esters within the polyurethane network contributes to achieving recyclability and reprocessability due to the dynamic characteristics of reversible boronic ester bonds [23].

Hence, in this work, we developed high-performance phosphorus/boron-containing polyurethane (PU-DP) elastomers with abundant dynamic borate ester bonds using poly(tetrahydrofuran) as a soft segment, a phosphorus-containing diol (DPDF) and isophorone diisocyanate as hard segments, and boric acid as a cross-linking agent. The chemical structure, transmittance, thermal stability, mechanical and adhesive properties, flame retardancy, physical recyclability, and shape-memory performances of PU-DP elastomers were studied comprehensively. In addition, the flame-retardant modes-of-action of PU-DP elastomers in the gas and condensed phases were investigated by different tests.

2. Experiment section

2.1. Materials

Dibutyltin dilaurate (DBTDL, 98 %), *N, N*-dimethylacetamide (DMAc, 99.8 %), poly(tetrahydrofuran) (PTMEG, number average molecular weight: ~2000), isophorone diisocyanate (IPDI, 98 %), boric

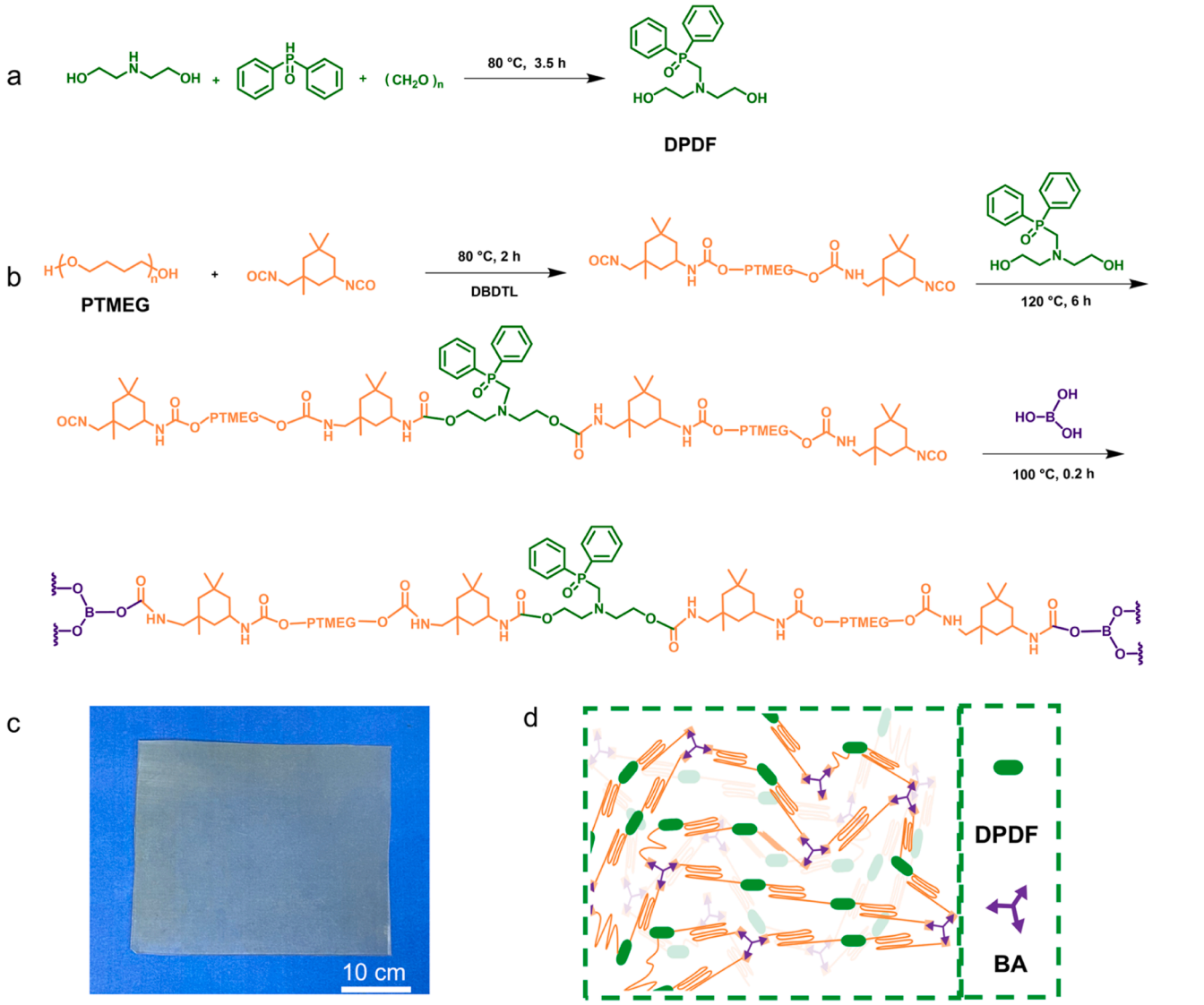

Fig. 1. (a) Synthesis route of DPDF, (b) preparation route of PU-DP elastomers, (c) digital image of PU-DP film, and (d) schematic diagram of PU-DP network.

acid (98 %), paraformaldehyde (96 %), diethanolamine (98 %) and diphenylphosphine oxide (DPPO, 98 %) were provided by Sarn Chemical Technology Co., Ltd. (Shanghai, China). All chemicals were used directly without further purification.

2.2. Synthesis of a phosphorus-containing diol (DPDF)

The synthesis of DPDF was based on a previous work [24], as shown in Fig. 1a. Diethanolamine (10.62 g, 100 mmol) and paraformaldehyde (3.19 g, 102 mmol) were introduced into a single-necked flask, which was equipped with a magnetic stirrer and a nitrogen inlet. The mixture was stirred at 80 °C under nitrogen atmosphere for 1 h to form a transparent solution, and then diphenylphosphine (20.63 g, 100 mmol) was added at this temperature and stirred for 3 h The resulting crude product was transferred to a vacuum oven and dried under reduced pressure at 90 °C for 6 h to obtain liquid DPDF.

2.3. Synthesis of the phosphorus/boron/nitrogen-containing PU (PU-DP) elastomers

The synthesis process of PU-DP is illustrated in Fig. 1b, and its formulation is shown in Table 1. PTMEG was firstly dried in a vacuum oven at 100 °C for 2 h PTMEG (10 g, 5 mmol), IPDI (4.45 g, 20 mmol), and DBTDL (1 or 2 drops) were added to a three-necked glass flask, and the mixture was stirred at 80 °C for 2 h under N_2 atmosphere. DPDF (2.6 g, 6.25 mmol) was dissolved in 20 mL of dry DMAc, and the resulting solution was added to the flask and stirred at 120 °C under N_2 atmosphere for 6 h Then, a DMAc solution (10 mL) containing boric acid (0.36 g, 5.83 mmol) was added to the flask and stirred for 15 min. The obtained solution was poured into a container and cured in an oven at 90 °C for 10 h to obtain a yellow transparent film (see Fig. 1c and d). PTMEG was used as the soft segments, and IPDI and DPDF were applied as the hard segments. For PU-DP 1–5, PU-DP 1–7, and PU-DP 1–9, the molar ratios of their soft segments to hard segments were 1:5, 1:7, and 1:9, and the molar ratio of -OH to -NCO was 1:1. The PUBC sample without DPDF was prepared by the same method as the PU-DP samples, and its molar ratio of soft segment to hard segment was the same as that of PU-DP 1–7 (1:7).

2.4. Characterization

The chemical structures of different raw materials and products were characterized by ^1H and ^{31}P nuclear magnetic resonance spectroscopy (NMR, DD2 400-MR, Agilent, USA), and DMSO-d_6 was used as a solvent. The FTIR spectra were recorded on a Nicolet 6700 spectrometer (Thermo Fisher, USA) with KBr pellets. The transmittance of PU-DP films (thickness: 0.20 ± 0.02 mm) was investigated by an ultraviolet-visible (UV–vis) spectroscope (Lambda35, PerkinElmer, USA). XPS was applied to investigate the chemical components of PU-DP 1–7 and its char on a Leybold instrument (Thermo Fisher Company, USA) with Al Ka radiation (1486.6 eV). The surface morphology and phosphorus and boron distribution of PU-DP 1–7 were investigated using a scanning electron microscope (SEM, Gemini SEM 300, Carl Zeiss, Germany) equipped with an energy dispersive X-ray spectroscope (EDX).

The tensile properties of PU-DP films (dumbbell-shaped, size: 0.8 mm × 4.0 mm × 50) were investigated by a universal testing machine (INSTRON 5966, USA) at a speed of 50 mm/min. The single-lap shear strengths of PU-DP 1–7 towards different substrates were investigated on the above machine at a speed of 5 mm/min based on ASTM D316. The results reported were the average of five samples. The cyclic tensile behaviors of PU-DP 1–7 sample with the size of 0.8 mm × 4.0 mm × 50 mm were investigated by the above machine at a strain rate of 50 mm/min. The experiments involved a cyclic stretching procedure with strain levels ranging from 50 % to 500 %.

Thermogravimetric analysis (TGA) was performed using a Q600SDT thermogravimetric analyzer (Netzsch, Germany). The test conditions include air/nitrogen condition, heating rate of 10℃/min, and test temperature of 30–800 ℃.

Dynamic mechanical analysis (DMA) was conducted by using a Q800 instrument (TA Instruments, USA) with a ramp-up of 3 °C/min at a frequency of 1 Hz in N_2 condition. Stress relaxation behaviors of PU-DP 1–7 (dimension: 30.0 mm × 6.0 mm × 1.0 mm) were carried out on the same instrument. A pre-loading force (0.001 N) was applied to the specimen, and the specimen was stabilized at the testing temperature for 10 min. The specimen was then stretched by 1.0 %, and the strain was maintained during the test. The relaxation modulus of the specimen was recorded.

Based on ASTM D3801, the UL-94 rating of the specimens (dimension: 120 mm × 13.0 mm ×3.0 mm) was determined by a Jiangning CFZ-3 equipment (China). In accordance with ASTM D2863, the LOI of the specimens was recorded using a Jiangning JF-3 oxygen index apparatus (China), and the specimen size was 100 mm × 6.5 mm ×3.0 mm. Cone calorimetry test (CCT) was conducted on a Yangyi VOUCH 6810 equipment under an external flux of 35 kW/m^2 based on ISO 5660. The specimen size was 100 mm × 100 mm ×3.0 mm. Microcalorimeter (FTT, UK) was also applied to investigate the flame retardancy of the specimens (powdered, ~5.0 mg).

Thermogravimetric analysis/infrared spectrometry (TG-IR) was conducted by a TGA2 (METTLER TOLEDO, Switzerland) integrated with a TENSORII spectrometer (BRUKER, Germany). The powdered specimen (~8 mg) was heated from 30 to 800 °C at a ramp-up of 20 °C /min under nitrogen atmosphere.

3. Results and discussion

3.1. Characterization of DPDF and PU-DP

The ^1H and ^{31}P NMR spectra of DPDF are presented in Fig. S1. In the ^1H NMR spectrum, the signals between 7.8 and 7.2 ppm belong to the protons of benzene ring, and those at 4.5, 3.8, 3.4, and 2.7 ppm are assigned to the protons of -OH, -P-CH_2-, -CH_2-O-, and -N-CH_2- groups, respectively. Notably, the chemical shift of P-H group at 8.7 ppm can be observed in the ^1H spectrum of DPPO, which disappears in the ^1H spectrum of DPDF. Additionally, there is only one peak at 26.9 ppm in the ^{31}P NMR spectrum of DPDF. All these results confirm the successful synthesis of DPDF.

The chemical structures of PU-DP elastomers were investigated using FTIR and XPS. The FTIR spectra of PU-DP elastomers and their building blocks are shown in Fig 2a and b. There is no characteristic absorption peak at 2250 cm^{-1} in the FTIR spectra of elastomers, indicating that the N=C=O group had been completely reacted [25]. The characteristic peaks at 3500 cm^{-1} for -OH (DPDF and PTMEG) and 3250 cm^{-1} for B-OH also vanished, confirming their participation in the reaction process. Furthermore, the peaks at 3310, 2920, 2850, 1700, 1243, and 695

Table 1
The formulations of PU-DP and PUBC elastomers.

Sample	PTMEG (mmol)	IPDI (mmol)	DPDF (mmol)	Boric acid (mmol)	PTMEG (wt%)	IPDI (wt%)	DPDF (wt%)	Boric acid (wt%)
PUBC	3	21	0	12	52.6	40.9	0	6.5
PU-DP 1–5	5	20	5	6.67	60.8	27.0	9.7	2.5
PU-DP 1–7	5	25	10	6.67	52.1	29.0	16.7	2.2
PU-DP 1–9	5	30	15	6.67	45.7	30.5	21.9	1.9

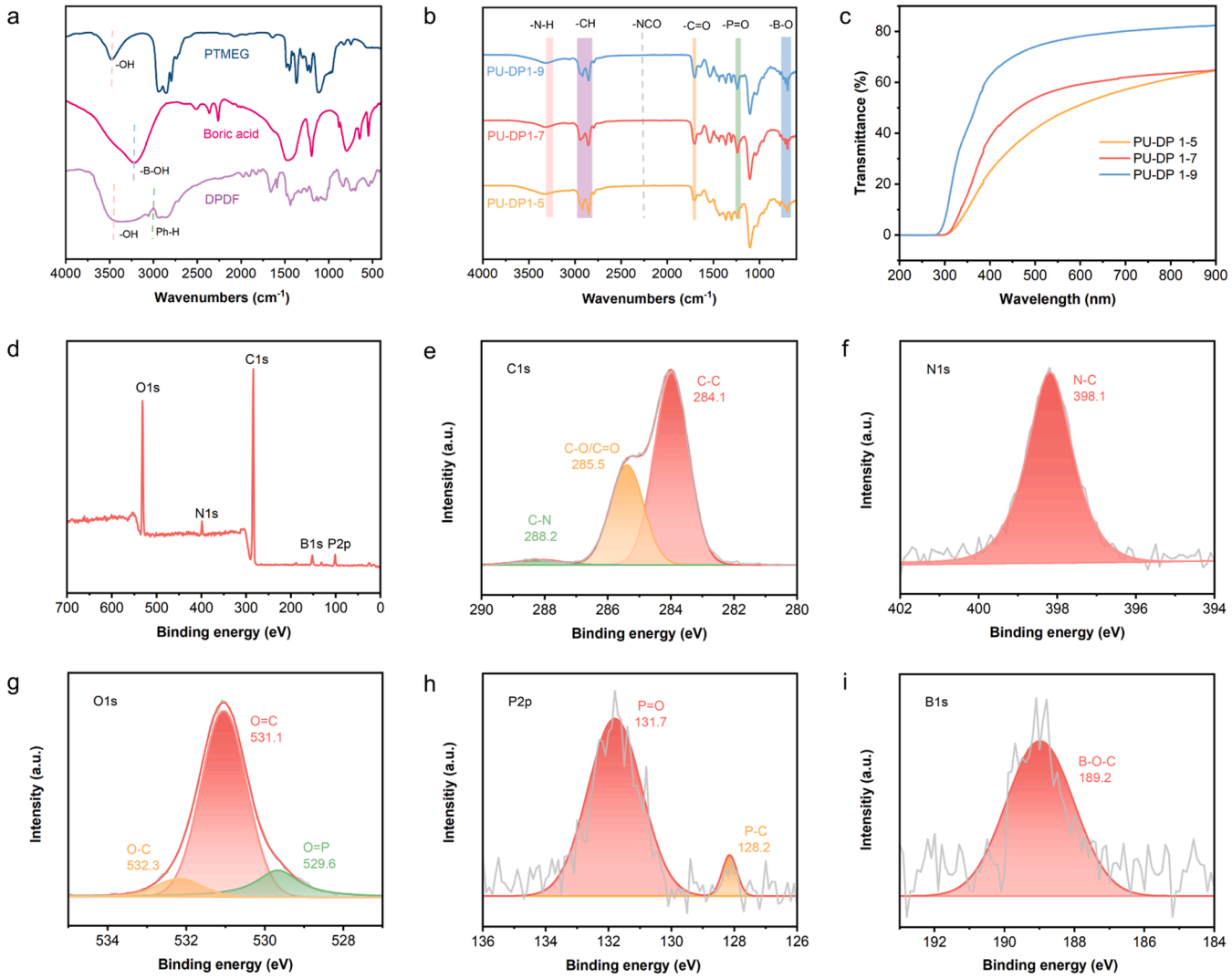

Fig. 2. (a) FTIR spectra of PTMEG, boric acid, and DPDF, (b) FTIR spectra of PU-DP 1–5, PU-DP 1–7, and PU-DP 1–9, (c) UV–vis transmission spectra of PU-DP films, (d) XPS full-scan spectrum of PU-DP 1–7, and XPS high-resolution (e) C1s, (f) N1s, (g) O1s, (h) P2p, and (i) B1s spectra of PU-DP 1–7.

cm^{-1} are attributed to the -NH, -CH=, -CH_2-, -C=O, -P=O, and -B-O groups [23,24]. These results confirm the existence of phosphorus, nitrogen, and boron within PU-DP network. The reaction between IPDI and boric acid was also confirmed by ^{1}H NMR. The reaction equation and the ^{1}H NMR spectra of the reaction product (BI), IPDI and boric acid are shown in Fig. S2. Compared with IPDI and boric acid, BI shows new chemical shifts between 5.5–6.7 ppm due to the protons of newly formed -NH- groups, demonstrating the reaction between IPDI and boric acid. Thus, boric acid can serve as a crosslinker in PU-DP system.

The transparency of PU-DP films was investigated by UV–vis testing, with the spectra shown in Fig. 2c. The transmittance of PU-DP 1–9 film reaches 80 % at the wavelength between 800 to 900 nm, demonstrating good transparency. The transmittance of both PU-DP 1–5 and PU-DP 1–7 is about 60 % at the wavelength of 900 nm. Due to the ultraviolet shielding effect of diphenyl group in DPPO, the transmittance of PU-DP films between 200 to 400 nm decreases with increasing DPPO content [26]. The XPS full-scan and high-resolution C1s, O1s, N1s, P2p, and B1s spectra of PU-DP 1–7 are shown in Fig. 2d-i. The C1s spectrum of PU-DP 1–7 demonstrates the deconvoluted peaks at 284.1 (C-C), 285.5 (C=O/C-O), and 288.2 (-C-N) eV. The O1s spectrum shows the peaks at 529.6 (O=P), 531.1(O=C), and 532.3 (O-C) eV. The P2p spectrum displays the peaks at 131.7 (P=O) and 128.2 (P-C) eV, and the N1s and B1s spectra show the peaks at 398.1 (N-C) and 189.2 (B-O-C) eV [27-29], respectively. The surface morphology of PU-DP 1–7 is shown in Fig. S3a, and the distribution of phosphorus and boron on its surface is displayed in Fig. S3b and c. The surface of PU-DP 1–7 film is continuous and intact, and phorsphorus and boron elements are evenly dispersed, confirming the formation of uniform crosslinking network. Based on these analyses, the P/N/B-containing PU-DP elastomers were successfully prepared in this work.

3.2. *Mechanical performances of PU-DP samples*

As shown in Fig. 3a, the glass transition temperature (T_g) values of PU-DP 1–5, PU-DP 1–7, and PU-DP 1–9 are -57.1, -57.9, and -53.5 °C, respectively. Since the PU-DP 1–9 sample contains the highest hard segment content among all samples, it shows the highest T_g and storage modulus at 25 °C (see Fig. 3b). According to previous works [30,31], the crosslinking density (V) of PU-DP elastomers was calculated, with the results shown in Table 2. The cross-linking density of PU-DP 1–5 is 36 mol/m^3. With the increase of the hard segment content, the cross-linking density of PU-DP samples shows an increasing trend, which may be because of the enhanced π-π stacking between DPDF parts. Obviously, the increase in the cross-linking density also leads to the increase in the T_g of PU-DP samples (see Table 2).

As shown in Fig. 3c and d, the PU-DP elastomers show high tensile

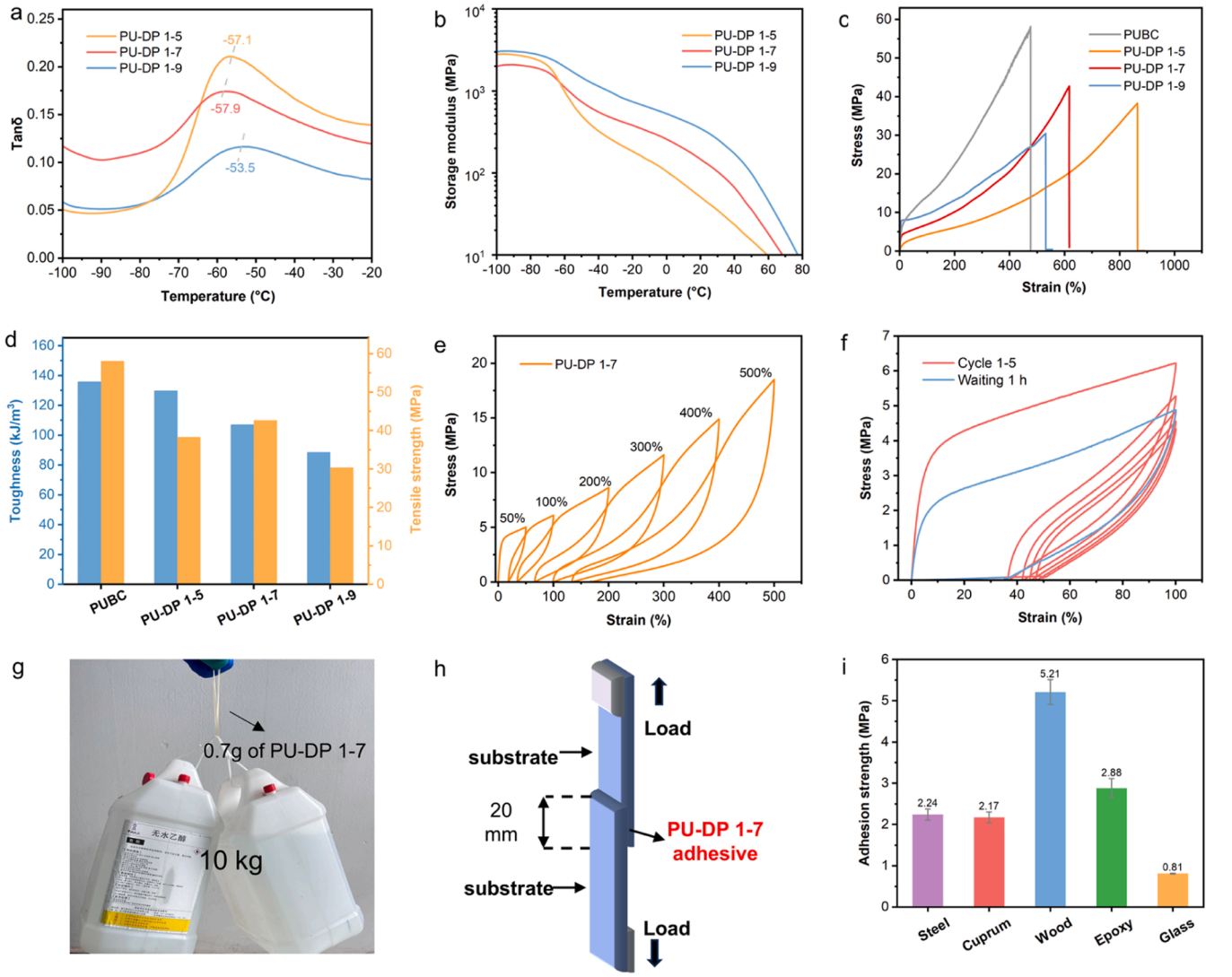

Fig. 3. (a) Tan δ and (b) storage modulus curves of PU-DP 1–5, PU-DP 1–7, and PU-DP 1–9, (c) tensile stress-strain curves of PUBC, U-DP 1–5, PU-DP 1–7, and PU-DP 1–9, (d) tensile toughness and strength of PUBC, PU-DP 1–5, PU-DP 1–7, and PU-DP 1–9, (e) cyclic tensile stress-strain plots of PU-DP 1–7 under different strains, (f) cyclic tensile stress-strain plots of PU-DP 1–7 under 100 % strain, (g) the digital photo of PU-DP 1–7 specimen loaded with 10 kg item, (h) schematic illustration of single lap shear test, and (i) adhesion strengths of PU-DP 1–7 on different substrates.

Table 2
Mechanical properties of PUBC and PU-DP samples.

Sample	T_g (°C)	V (mol/m^3)	Molar ratio of soft to hard segments	Tensile strength (MPa)	Elongation at break (%)	Toughness (kJ/m^3)
PUBC	/	/	1–7	58.1 ±4.5	476.3 ±44.0	135.8±6.3
PU-DP 1–5	-57.1	36	1–5	38.2 ±1.7	890.6 ±17.0	129.7±5.7
PU-DP 1–7	-57.9	71	1–7	41.8 ±1.5	657.3 ±50.3	106.9±3.8
PU-DP 1–9	-53.5	127	1–9	29.7 ±1.3	516.9 ±23.7	88.6±4.0

strength and toughness. In detail, PU-DP 1–7 features a tensile strength of 42.7 MPa, an elongation at break of 616.9 %, and a tensile toughness of 106.9 kJ/m^3 (see Table 2). With the increase of IPDI and DPDF contents, the π-π stacking between DPDF parts are enhanced and the cross-linking density of PU-DP elastomer is increased, leading to the increased rigidity and thus the decreased elongation at break and toughness. Compared with PUBC, the PU-DP 1–7 elastomer shows comparable mechanical properties, suggesting that the introduction of DPDF does not significantly affect the mechanical performances. The cyclic tensile test was conducted on PU-DP 1–7 sample to study its self-recovery ability [32]. The cyclic tensile stress-strain curves of PU-DP 1–7 under different strains (50 %-500 %) are shown in Fig. 3e, and those under 100 % strain for different cycles are displayed in Fig. 3f. In Fig. 3e, the hysteresis loop and dissipated energy increase gradually with increasing tensile strain. Under the constant strain of 100 %, the hysteresis area reduces as the tensile cycle increases (see Fig. 3f). When the recovery time prolongs to 1 h, the stress-strain curve is close to that of the first cycle, indicative of the time-dependent self-recovery ability of PU-DP 1–7. During stretching, abundant hydrogen bonds within the PU-DP 1–7 network are broken and reformed, leading to the dissipation of energy, thus achieving great mechanical properties [28,33-35]. In addition, 0.7 g of the rectangular PU-DP 1–7 sample (size: 100 mm × 5 mm × 0.7 mm) can lift a 10 kg item without breaking (see Fig. 3 g), further demonstrating its great mechanical properties.

Polyurethane is widely used as coating and adhesive in various industries due to its excellent adhesive properties [26,36]. Hence, we

conducted the single lap shear tests of PU-DP 1–7 on steel, cuprum, wood, epoxy resin (EP), and glass substrates, respectively. The specimens were prepared by fixing the PU-DP 1–7 mixture between the substrates and curing it at 90 °C for 4 h (see Fig. 3h). As presented in Fig. 3i, the adhesive strengths of PU-DP 1–7 to steel, cuprum, wood, EP, and glass are 2.24, 2.17, 5.21, 2.88, and 0.81 MPa, respectively. These results demonstrate that PU-DP 1–7 exhibits great mechanical and adhesive properties because its network contains a great deal of hydrogen bonds, making it suitable for various applications [28].

3.3. Thermal stability of PU-DP samples

The thermal stability of PU-DP samples in air and N_2 conditions was studied by TGA. The thermogravimetric (TG) and derivative TG (DTG) curves of PU-DP samples are shown in Fig. S4, and the corresponding thermal stability data are listed in Table S1, including the temperature at 5 % weight loss ($T_{5\,\%}$), the temperature at the maximum weight loss rate (T_{max1} and T_{max2}), and the char yield at 800 °C (*CY*). In air condition, the $T_{5\,\%}$ and T_{max1} of PU-DP 1–5 are 259 and 403 °C, and those of PU-DP 1–9 are decreased to 245 and 387 °C, which is probably because of the catalytic decomposition effect of phosphorus-containing group. Compared with PU-DP 1–5 (0.8 %), the *CY* of PU-DP 1–9 is increased to 2.0 %, indicating the promoting carbonization effect of P-containing group.

Under N_2 atmosphere, the PU-DP sample shows two decomposition stages: the first stage is attributed to the decomposition of P-containing group and the cleavage of carbamate [37], and the second stage is assigned to the gradual decomposition of polyols and carbonyls in the soft segment [24]. In nitrogen condition, the $T_{5\,\%}$, T_{max1} and T_{max2} of PU-DP 1–5 are 266, 323 and 425 °C, respectively, and these values are gradually decreased with increasing phosphorus content. In addition, the *CY* increases from 2.3 % of PU-DP 1–5 to 3.2 % of PU-DP 1–9. Hence, the introduction of P-containing group reduces the initial decomposition temperature of PU-DP samples but enhances the char-forming ability.

3.4. Flame retardancy of PU-DP samples

The LOI and UL-94 results of PUBC and PU-DP samples are shown in Fig. 4a and Table 3. The UL-94 tests of PUBC and PU-DP are recorded in Video S1-S4. The polyurethane elastomer is a class of highly flammable polymers and will generate lots of melting droplets during burning, thus its LOI is about 20 % and it cannot pass the UL-94 test [38]. Without the phosphorus element, the PUBC sample shows a low LOI of 19.5 % and it cannot pass the UL-94 test. As DPDF is introduced, the PU-DP samples

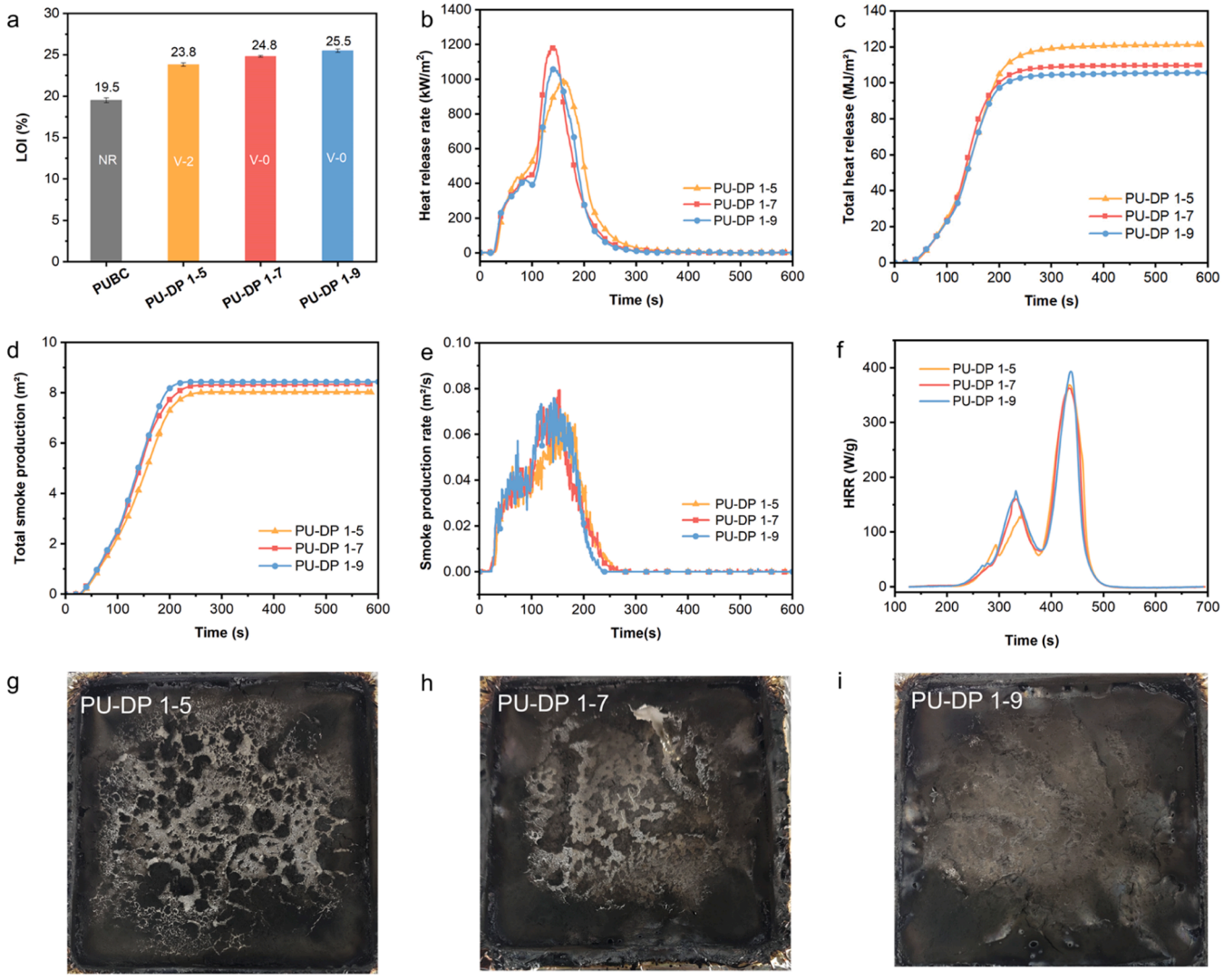

Fig. 4. (a) LOI and UL-94 rating of PUBC and PU-DP samples, (b) heat release rate, (c) total heat release, (d) total smoke production, and (e) smoke production rate curves of PU-DP samples obtained from CCT, (f) heat release rate curves of PU-DP samples obtained from MCC, and digital photographs of (g) PU-DP 1–5, (h) PU-DP 1–7, and (i) PU-DP 1–9 chars after cone calorimetry.

Table 3
The LOI and UL-94 rating of PUBC and PU-DP samples.

Sample	LOI (%)	UL-94 result (3 mm)		
		av-(t_1+t_2) [a] (s)	Dripping	Rating
PUBC	19.5	>90	Yes	NR
PU-DP 1–5	23.5	13.5±5.3	Yes	V-2
PU-DP 1–7	24.8	2.6±1.0	No	V-0
PU-DP 1–9	25.5	3.3±0.2	No	V-0

[a] t_1 represents the burning time after the first ignition, t_2 represents the burning time after the second ignition, and av-(t_1+t_2) is the average of t_1 and t_2 [39,40].

show higher LOI values and UL-94 ratings than PUBC sample. For instance, the PU-DP 1–5 sample passes a UL-94 V-2 rating and achieves an LOI of 23.5 %. With increasing P content, the burning time of PU-DP 1–7 and PU-DP 1–9 is shortened during UL-94 tests, and no droplets are generated. Therefore, PU-DP 1–7 and PU-DP 1–9 obtain a UL-94 V-0 classification, and their LOI values are up to 24.8 % and 25.5 %. PU-DP 1–9 with the highest P content shows the greatest flame retardancy.

The cone calorimetry test was conducted on PU-DP materials to further investigate the flame retardancy, with the results presented in Fig. 4b-e and Table 4. The time to ignition (TTI) of PU-DP 1–5 is 28 s, and that of PU-DP 1–9 is reduced to 25 s, further confirming the catalytic decomposition effect of P-containing group [41-43]. As shown in Fig. 4b and Table 4, the peak heat release rate (PHRR) values of all PU-DP samples are close. With the increase of P content, the total heat release (THR) decreases from 121.2 MJ/m^2 of PU-DP 1–5 to 105.7 MJ/m^2 of PU-DP 1–9 (see Fig. 4c), which demonstrates that the P-containing decomposition products from DPDF segments can suppress the heat release of the PU matrix during combustion. With the increase of P content, the total smoke production (TSP), peak smoke production rate (PSPR), and average CO yield (ACOY) of PU-DP samples gradually increase (see Fig. 4d and e and Table 4), and the average CO_2 yield (ACO_2Y) reduces, indicating the increased incomplete burning degree [44]. The digital images of char layers obtained from cone calorimetry tests are presented in Fig. 4 g-i. Clearly, the PU-DP 1–9 char is more compact and denser than other chars, further demonstrating the catalytic carbonization effect of P-containing group.

The micro-cone calorimetry (MCC) tests were also conducted on PU-DP samples. The peak heat release rate values of all PU-DP samples were about 370 W/g (see Fig. 4f). Meanwhile, with the increase of P content, the total heat release of PU-DP samples is gradually decreased, further confirming the positive effect of P-containing group on suppressing heat release during combustion.

3.5. Flame-retardant action in the condensed phase

To explore the flame-retardant mode-of-action of PU-DP in the condensed phase, X-ray photoelectron spectroscopy was used to analyze the chemical composition of the PU-DP 1–7 char residue after CCT. The PU-DP 1–7 char is composed of carbon, oxygen, nitrogen, phosphorus, and boron (see Fig. 5a). The C1s spectrum of PU-DP 1–7 char in Fig. 5b can be divided into two peaks at 285.3 and 284.2 eV, corresponding to C-C/N and C=O bonds, respectively. The N1s spectrum shows two peaks at 400.0 and 399.8 eV, which belong to -N-C and -NHCO structures. The O1s spectrum can be divided into two peaks, which are assigned to O-C (531.6 eV) and O=C/P (529.8 eV) structures, respectively. The P2p spectrum confirms the existence of P-C (134.8 eV) and P=O (133.5 eV) bonds [45], and the B1s spectrum displays a peak of -B-O/C structure at 192.3 eV [22]. In addition, the phosphorus and boron contents (9.3 and 15.2 wt%) of PU-DP 1–7 char are much higher than those (1.9 and 3.0 wt %) of PU-DP 1–7 sample (see Table S2), demonstrating that many phosphorus- and boron-containing decomposition products participate in the carbonization and promote the formation of a protective char layer on the PU surface to suppress the heat release and enhance the flame retardancy [41,42,46].

Table 4
Cone calorimetry results for PU-DP samples.

Sample	TTI (s)	PHRR (kW/m^2)	THR (MJ/m^2)	TSP (m^2)	PSPR (m^2/s)	ACOY (kg/kg)	ACO_2Y (kg/kg)
PU-DP 1–5	28	999.1	121.2	8.02	0.06	0.06	6.23
PU-DP 1–7	27	1191.3	109.6	8.34	0.07	0.11	5.99
PU-DP 1–9	25	1060.2	105.7	8.40	0.07	0.16	5.43

3.6. Flame-retardant action in the gas phase

TG-IR analyses were performed on PU-DP 1–7 and PU-DP 1–9 samples under N_2 atmosphere to study their gaseous products during thermal degradation, with the curves shown in Fig. 6. As presented in Fig. 6c, e and f, the main gas products of PU-DP 1–7 and PU-DP 1–9 samples during thermal decomposition include water (3738 cm^{-1}), hydrocarbons (2864 cm^{-1}), carbon dioxide (2354 cm^{-1}), carbonyl compounds (1740 cm^{-1}), aromatic hydrocarbons, (1464–1362 cm^{-1}), ether derivatives (1102 cm^{-1}), P-O-pH (920 cm^{-1}), and amino groups (727 cm^{-1}) [24,38]. It is worth noting that the thermal decomposition intensity of PU-DP 1–9 is less than that of PU-DP 1–7 (see Fig. 6a, b, and d), indicating that with increasing P content and crosslinking degree, the thermal decomposition products of PU-DP gradually decrease, and the char yield increases. Hence, the TG-IR results further confirm the promoting carbonization effect of P-containing group, which is conducive to flame retardancy.

3.7. Physical recycling

To investigate the physical recycling and reprocessing capabilities of PU-DP 1–7, it was segmented, and the obtained fragments were hot pressed at different temperatures for 20 min under 8 MPa to reform the films (see Fig. 7a and b) [31]. The tensile properties of the reformed PU-DP 1–7 films were investigated, with the stress-strain curves shown in Fig. 7c. The results prove that the PU-DP 1–7 film can be recycled. By hot-pressing the PU-DP 1–7 fragments at 140 °C, the complete film can be reproduced, of which the tensile strength and elongation at break are 75.3 % and 83.6 % of those of the original PU-DP 1–7 film, respectively (see Fig. 7d). When reducing the hot-pressing temperature to 130 °C, the intact PU-DP 1–7 film can still be remade. Obviously, the PU-DP 1–7 features recyclability and reprocessability due to the existence of abundant dynamic borate ester bonds. The performances of PU-DP 1–7 were compared with previous flame-retardant PU samples in Table S3. Compared with previous PU samples, our PU-DP 1–7 shows a higher tensile strength of 41.8 MPa due to the introduction of boric acid as a crosslinking agent. Meanwhile, incorporating boric acid also allows PU DP 1–7 to achieve reprocessability because of the formation of dynamic borate ester bonds.

Due to the presence of dynamic boronate bonds, the crosslinking network of PU-DP 1–7 can be rearranged when it is heated above the topological freezing transition temperature (T_v) [47-49]. Therefore, the T_v of PU-DP 1–7 and the activation energy (E_a) of boronic ester exchange reaction within PU-DP 1–7 network were studied by stress relaxation test. Fig. 7e shows the stress relaxation curves of PU-DP 1–7 at different temperatures. According to Maxwell's model, the relaxation time (τ) of a polymer is usually defined as the time for its modulus (G) to decrease to 1/e of the original modulus (G_0) [50]. For stress relaxation tests of PU-DP 1–7, the temperatures were set as 90, 110, and 130 °C, respectively. Obviously, the relaxation time decreases with increasing temperature, from 140 s (90 °C) to 5 s (130 °C). According to Fig. 7f, the relationship between testing temperature (T) and τ of PU-DP 1–7 follows

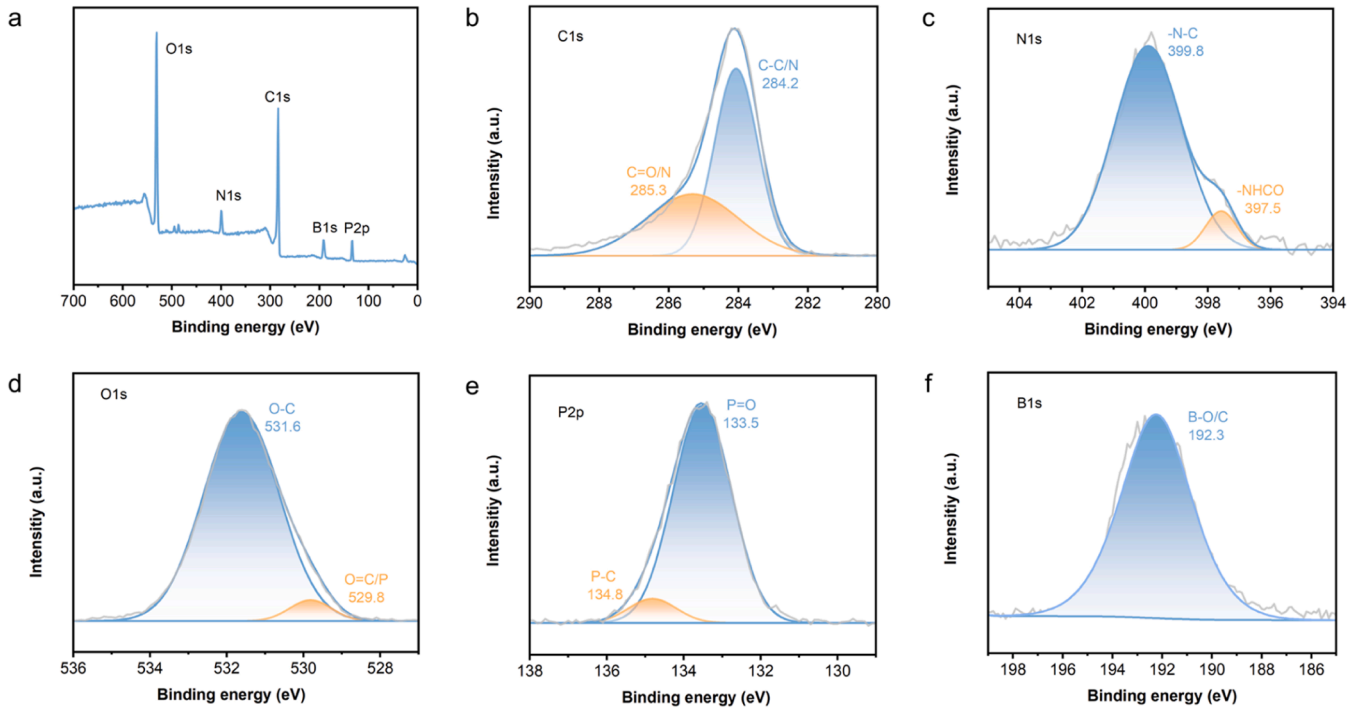

Fig. 5. (a) XPS spectrum of char residue for PU-DP 1–7, and XPS high-resolution (b) C1s, (c) N1s, (d) O1s, (e) P2p, and (f) B1s spectra of PU-DP 1–7 char after cone calorimetry test.

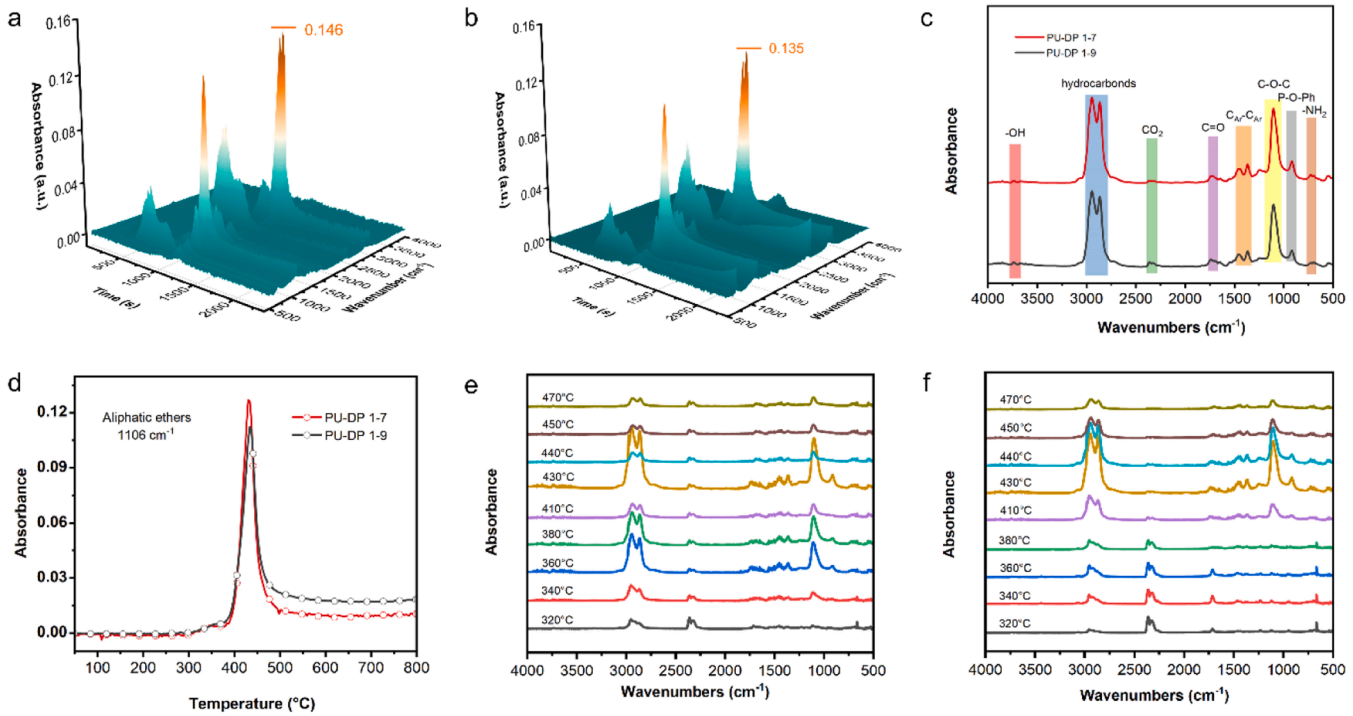

Fig. 6. 3D TG-IR spectra of pyrolysis products for (a) PU-DP 1–7 and (b) PU-DP 1–9, (c) FTIR spectra of gas decomposition products for PU-DP 1–7 and PU-DP 1–9 at T_{max1}, (d) absorbance *vs.* temperature plots of PU-DP 1–7 and PU-DP 1–9 at 1106 cm^{-1}, and FTIR spectra of gas decomposition products for (e) PU-DP 1–7 and (f) PU-DP 1–9 at different temperatures.

the Arrhenius Eq. (1) from 90–130 °C:

$$\ln\tau = \frac{E_a}{RT} - \ln A \quad (1)$$

where A is the preexponential factor, and R is 8.314 J mol^{-1} K^{-1}.

Through linear fitting (R^2 = 0.9799), the E_a of the boronic ester exchange reaction within the PU-DP 1–7 network is determined to be 107.38 kJ/mol, which is within the range of E_a value for boronic ester exchange reaction reported in previous works [31,48,49]. This result confirms that PU-DP 1–7 can undergo the boronic ester exchange

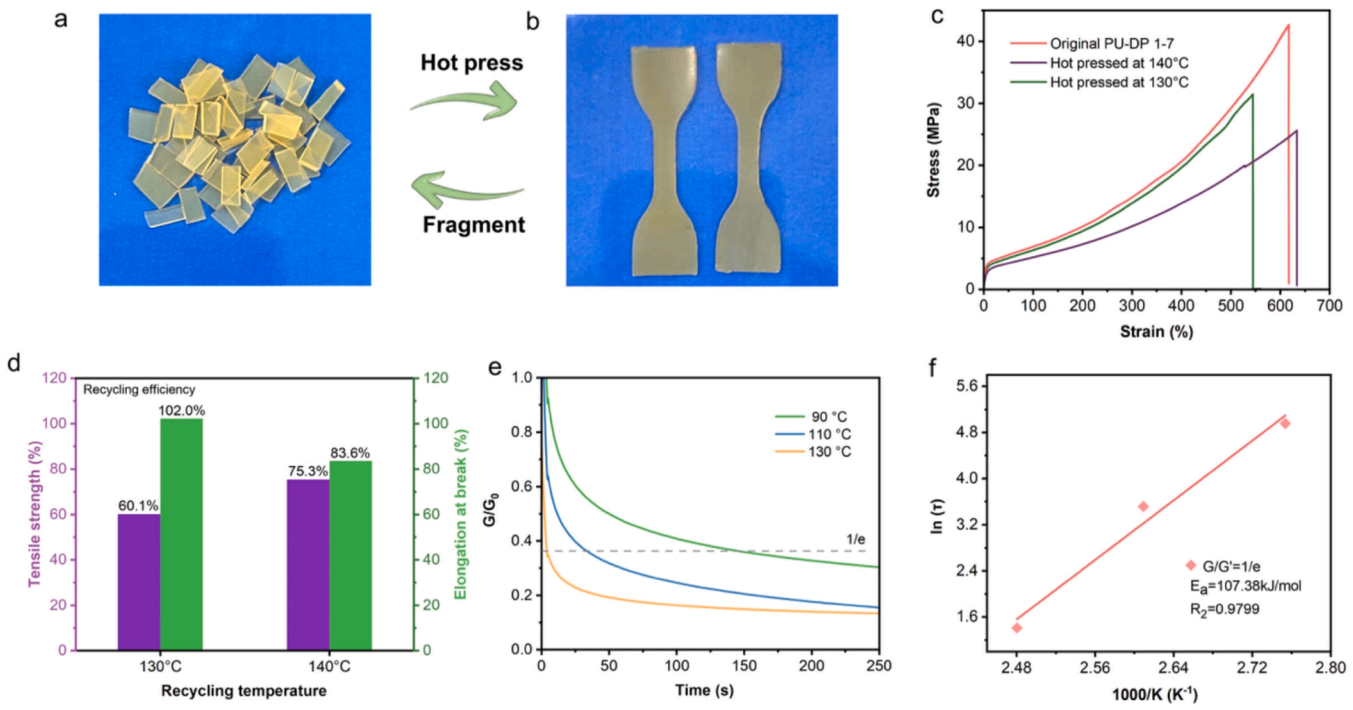

Fig. 7. The digital images of (a) PU-DP 1–7 fragments and (b) reformed PU-DP 1–7 specimens after hot-pressing, (c) tensile stress-strain curves of the reformed PU-DP 1–7 specimens, (d) recovery efficiency of the reformed PU-DP 1–7 sample at 140 ℃, (e) stress relaxation curves of PU-DP 1–7, and (f) the linear fitting curve of PU-DP 1–7 based on the Arrhenius equation.

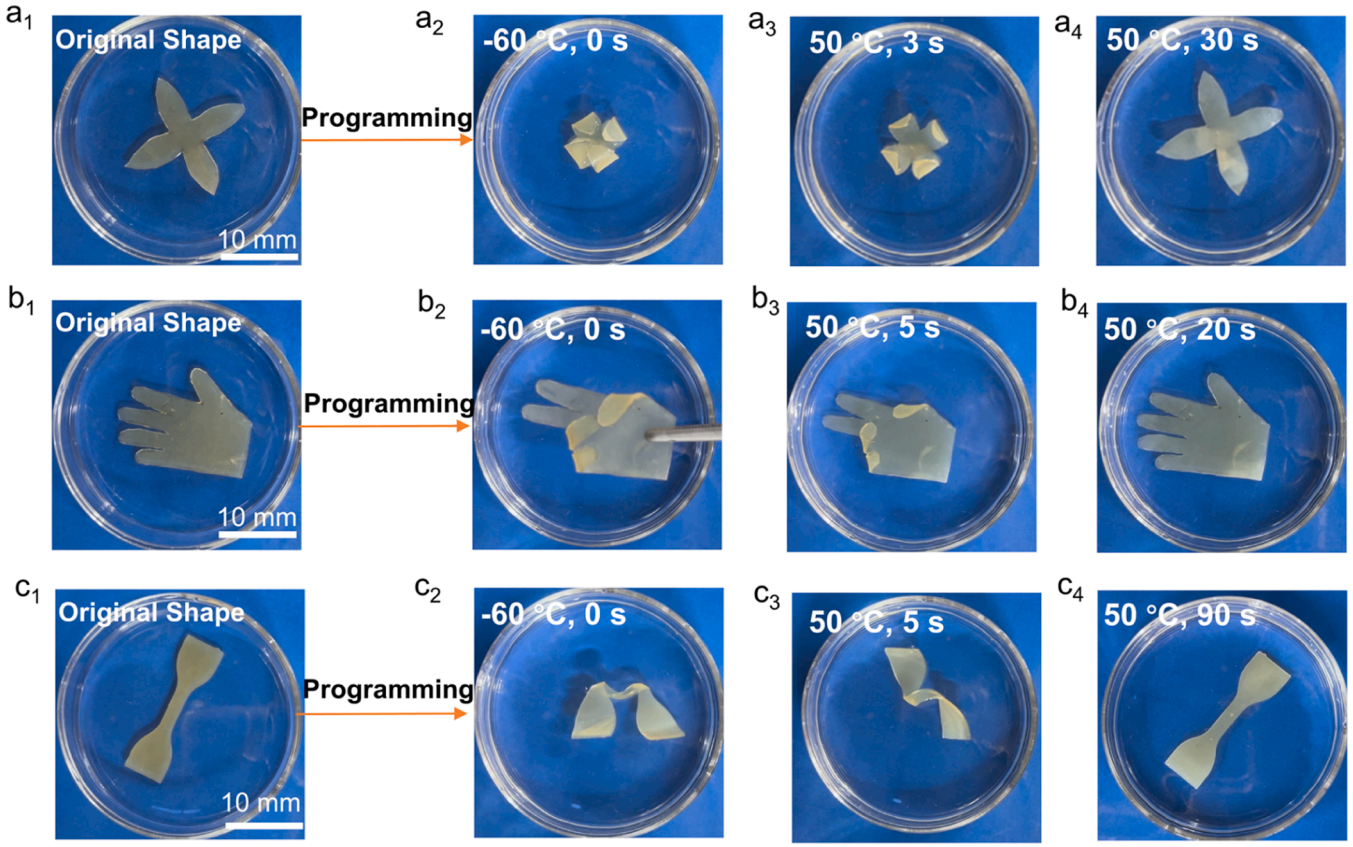

Fig. 8. Digital photographs of the shape memory process for PU-DP 1–7 specimens with different shapes: (a) four-leaf petal, (b) hand, and (c) dumbbell.

reaction under external stimulation, such as heat.

The T_v is the temperature at which the viscosity reaches 10^{12} Pa·s [49]. The relationship between the viscosity and modulus of a polymeric material follows the Eq. (2) and (3):

$$\eta = G_s \tau \tag{2}$$

$$G_s = \frac{E'}{2(1+\nu)} \tag{3}$$

where G_s is the estimated shear modulus, η is the viscosity of the material, E' is the storage modulus at the rubber plateau, ν is the Poisson's ratio, and τ is relaxation time [51-55].

According to the Eq. (1)-(3), the T_v of PU-DP 1–7 can be calculated to be 57.5 °C. All these results confirm that PU-DP 1–7 can be easily recycled in mild conditions due to abundant borate ester bonds in its network.

3.8. Shape memory properties

To demonstrate the shape memory ability of PU-DP 1–7, the samples were cut into different shapes, including four-leaf petal (see Fig. 8a), hand shape (see Fig. 8b), and dumbbell strip (see Fig. 8c). The obtained samples were programmed at room temperature and their shapes were then fixed at -60 °C for about 5 s, finally the samples were placed at 50 °C to recover. As shown in Fig. 8, all these specimens can recover to their original shapes after placing at 50 °C for different time, confirming the good shape memory properties of PU-DP 1–7. Obviously, the topological structure of PU-DP 1–7 can be rearranged under heating due to the exchangeable boronic ester bonds, thus exhibiting shape memory property [36,56,57].

4. Conclusion

In this study, we developed a flame-retardant polyurethane (PU-DP) elastomer based on dynamic borate esters, which exhibited good mechanical, shape memory, and physical recycling properties. Due to a large number of hydrogen bonds within the crosslinking network, PU-DP 1–7 shows a tensile strength of 42.7 MPa and an elongation at break of 616.9 %, with high adhesion strengths on different substrates. At the same time, the introduction of phosphorus and boron elements enables PU-DP 1–7 to achieve superior flame retardancy, as reflected by an LOI of 24.8 % and a UL-94 V-0 rating. Moreover, the dynamic boronic ester bonds endow PU-DP 1–7 with great reprocessing and shape-memory performances. This work provides an integrated design strategy for the development of flame-retardant, recyclable, and shape-memory polyurethane elastomers with high mechanical properties based on dynamic borate ester bonds, which are expected to be used as fire-retardant coatings and polymers in different industries.

CRediT authorship contribution statement

Tiantian Zhang: Writing – original draft, Visualization, Investigation, Conceptualization. **Siqi Huo:** Writing – review & editing, Supervision, Project administration, Conceptualization. **Guofeng Ye:** Resources, Investigation. **Cheng Wang:** Visualization. **Qi Zhang:** Validation. **Yijiao Xue:** Supervision. **Pingan Song:** Supervision. **Hao Wang:** Supervision. **Zhitian Liu:** Supervision, Project administration.

Declaration of competing interest

The authors declare that they have no known competing financial interests or personal relationships that could have appeared to influence the work reported in this paper.

Acknowledgments

This work was supported by the Australian Research Council (DE230100616), and Wuhan Institute of Technology Graduate Innovation Education Fund (CX2023100).

Supplementary materials

Supplementary material associated with this article can be found, in the online version, at doi:10.1016/j.polymdegradstab.2024.111047.

Data availability

Data will be made available on request.

References

[1] Y. Xia, Y. He, F. Zhang, Y. Liu, J. Leng, A review of shape memory polymers and composites: Mechanisms, materials, and applications, Adv. Mater. 33 (6) (2021) 2000713, https://doi.org/10.1002/adma.202000713.
[2] M. Zare, M.P. Prabhakaran, N. Parvin, S. Ramakrishna, Thermally-induced two-way shape memory polymers: mechanisms, structures, and applications, Chem. Eng. J. 374 (2019) 706–720, https://doi.org/10.1016/j.cej.2019.05.167.
[3] X.M. Liu, Mechanical response of composite materials prepared with polyurethane elastomers and polyvinyl chloride films, J. Mech. Behav. Biomed. Mater. 146 (2023) 106006, https://doi.org/10.1016/j.jmbbm.2023.106006.
[4] J. Herzberger, J.M. Sirrine, C.B. Williams, T.E. Long, Polymer design for 3D printing elastomers: recent advances in structure, properties, and printing, Prog. Polym. Sci. 97 (2019) 101144, https://doi.org/10.1016/j.progpolymsci.2019.101144.
[5] Y. Cao, R. Yan, X. Wo, J. Ma, X. Yu, A. Li, J. Huang, F. Li, Q. Zhang, A self-healing elastomer with outstanding mechanical properties was designed based on urea bonds, J. Mater. Chem. C 12 (26) (2024) 9685–9692, https://doi.org/10.1039/d4tc01123f.
[6] S. Peng, N. Thirunavukkarasu, J. Chen, X. Zheng, C. Long, X. Huang, Z. Weng, L. Zheng, H. Wang, X. Peng, L. Wu, Vat photopolymerization 3D printing of transparent, mechanically robust, and self-healing polyurethane elastomers for tailored wearable sensors, Chem. Eng. J. 463 (1) (2023) 142312, https://doi.org/10.1016/j.cej.2023.142312.
[7] B. Jia, H. Huang, Z. Dong, X. Ren, Y. Lu, W. Wang, S. Zhou, X. Zhao, B. Guo, Degradable biomedical elastomers: paving the future of tissue repair and regenerative medicine, Chem. Soc. Rev. 53 (8) (2024) 4086–4153, https://doi.org/10.1039/d3cs00923h.
[8] Y. Yu, Z. Xu, L. Xu, Y. Li, T. Liu, Q. Meng, X. Su, H.C. Kuan, J. Dai, J. Ma, Highly stretchable, sensitive and healable polyurethane-urea/graphene nanocomposite sensor for multifunctional applications, Thin-Walled Struct 198 (2024) 111660, https://doi.org/10.1016/j.tws.2024.111660.
[9] P.Y. Siboro, A.K. Sharma, P.J. Lai, J. Jayakumar, F.L. Mi, H.L. Chen, Y. Chang, H. W. Sung, Harnessing HfO_2 nanoparticles for wearable tumor monitoring and sonodynamic therapy in advancing cancer care, ACS Nano 18 (3) (2024) 2485–2499, https://doi.org/10.1021/acsnano.3c11346.
[10] Y. Xue, J. Lin, T. Wan, Y. Luo, Z. Ma, Y. Zhou, B.T. Tuten, M. Zhang, X. Tao, P. Song, Stretchable, ultratough, and intrinsically self-extinguishing elastomers with desirable recyclability, Adv. Sci. 10 (9) (2023) 2207268, https://doi.org/10.1002/advs.202207268.
[11] C.S. Wang, J. Zhang, H. Wang, M. He, L. Ding, W.W. Zhao, Simultaneously improving the fracture toughness and flame retardancy of soybean oil-based waterborne polyurethane coatings by phosphorus-nitrogen chain extender, Ind. Crops Prod. 163 (2021) 113328, https://doi.org/10.1016/j.indcrop.2021.113328.
[12] Y. Xue, T. Zhang, H. Peng, Z. Ma, M. Zhang, M. Lynch, T. Dinh, Z. Zhou, Y. Zhou, P. Song, Fire-retardant, anti-dripping, biodegradable and biobased polyurethane elastomers enabled by hydrogen-bonding with cellulose nanocrystals, Nano Res 17 (2024) 2186–2194, https://doi.org/10.1007/s12274-023-6397-0.
[13] X. Du, L. Jin, S. Deng, M. Zhou, Z. Du, X. Cheng, H. Wang, Recyclable, self-healing, and flame-retardant solid–solid phase change materials based on thermally reversible cross-links for sustainable thermal energy storage, ACS Appl. Mater. Interfaces 13 (36) (2021) 42991–43001, https://doi.org/10.1021/acsami.1c14862.
[14] J.R. Xavier, S.P. Vinodhini, B. Ramesh, Optimizing aluminum alloy performance for marine superstructures: Advanced nanocomposite coating for enhanced corrosion resistance, flame retardancy, and mechanical strength, Polym. Degrad. Stab. 227 (2024) 110847, https://doi.org/10.1016/j.polymdegradstab.2024.110847.
[15] J.R. Xavier, S.P. Vinodhini, J. Raja Beryl, Anti-corrosion and flame-retardant properties of environmentally benign smart functionalized WS2/rGO in epoxy coatings for enhanced steel structural protection in natural seawater, Mater. Today Commun. 38 (2024) 107842, https://doi.org/10.1016/j.mtcomm.2023.107842.
[16] J.R. Xavier, Multifunctional nanocomposite coatings for superior anticorrosive, flame retardant and mechanical properties in aerospace components, Surf. Interfaces 38 (2023) 102832, https://doi.org/10.1016/j.surfin.2023.102832.

[17] J.R. Xavier, Investigation of anticorrosion, flame retardant and mechanical properties of polyurethane/GO nanocomposites coated AJ62 Mg alloy for aerospace/automobile components, Diamond Relat. Mater. 136 (2023) 110025, https://doi.org/10.1016/j.diamond.2023.110025.
[18] G. Ye, S. Huo, C. Wang, Q. Zhang, H. Wang, P. Song, Z. Liu, Strong yet tough catalyst-free transesterification vitrimer with excellent fire-retardancy, durability, and closed-loop recyclability, Small (2024) 2404634, https://doi.org/10.1002/smll.202404634.
[19] X. Cao, J. Huang, Z. Tang, Y. Tong, A.C.Y. Yuen, W. Zhao, Q. Huang, R.K.Y. Li, W. Wu, Self-assembled biobased chitosan hybrid carrying N/P/B elements for polylactide with enhanced fire safety and mechanical properties, Int. J. Biol. Macromol. 236 (1) (2023) 123947, https://doi.org/10.1016/j.ijbiomac.2023.123947.
[20] Q. Chen, S. Huo, Y. Lu, M. Ding, J. Feng, G. Huang, H. Xu, Z. Sun, Z. Wang, P. Song, Heterostructured graphene@ Silica@ iron phenylphosphinate for fire-retardant, strong, thermally conductive yet electrically insulated epoxy nanocomposites, Small 31 (20) (2024) 2310724, https://doi.org/10.1002/smll.202310724.
[21] J. Wang, J. Wang, S. Yang, X. Chen, K. Chen, G. Zhou, X. Liu, L. Xu, S. Huo, P. Song, H. Wang, Multifunctional phosphorus-containing imidazoliums endowing one-component epoxy resins with superior thermal latency, heat resistance, mechanical properties, and fire safety, Chem. Eng. J. 485 (2024) 149852, https://doi.org/10.1016/j.cej.2024.149852.
[22] G. Ye, S. Huo, C. Wang, Q. Shi, L. Yu, Z. Liu, Z. Fang, H. Wang, A novel hyperbranched phosphorus-boron polymer for transparent, flame-retardant, smoke-suppressive, robust yet tough epoxy resins, Composites, Part B 227 (15) (2021) 109395, https://doi.org/10.1016/j.compositesb.2021.109395.
[23] C. Bao, X. Zhang, P. Yu, Q. Li, Y. Qin, Z. Xin, Facile fabrication of degradable polyurethane thermosets with high mechanical strength and toughness via the cross-linking of triple boron–urethane bonds, J. Mater. Chem. A 9 (39) (2021) 22410–22417, https://doi.org/10.1039/d1ta06314f.
[24] J. Choi, K.H. Min, B.S. Kim, S.H. Baeck, S.E. Shim, Y. Qian, Preparation of Ar–P–N-structured flame retardant via Kabachnik–Fields reaction for fire safety and mechanical reinforcement of polyurethane, Prog. Org. Coat. 186 (2024) 108081, https://doi.org/10.1016/j.porgcoat.2023.108081.
[25] Z. Zhang, L. Qian, G. Huang, C. Chen, J. Cheng, X. Yao, C. Ma, G. Zhang, Insertion of urea moieties for one-component strong yet tough, self-healing polyurea protective materials, Adv. Funct. Mater. 34 (2023) 2310603, https://doi.org/10.1002/adfm.202310603.
[26] C. Wang, S. Huo, G. Ye, P. Song, H. Wang, Z. Liu, A P/Si-containing polyethylenimine curing agent towards transparent, durable fire-safe, mechanically-robust and tough epoxy resins, Chem. Eng. J. 451 (1) (2023) 138768, https://doi.org/10.1016/j.cej.2022.138768.
[27] X. Shang, Y. Jin, W. Du, L. Bai, R. Zhou, W. Zeng, K. Lin, Flame-retardant and self-healing waterborne polyurethane based on organic selenium, ACS Appl. Mater. Interfaces 15 (12) (2023) 16118–16131, https://doi.org/10.1021/acsami.3c02251.
[28] Y. Song, J. Li, G. Song, X. Li, Tough and self-healing waterborne polyurethane elastomers via dynamic hydrogen bonds design for flexible conductive substrate applications, ACS Appl. Mater. Interfaces 16 (2) (2024) 2683–2691, https://doi.org/10.1021/acsami.3c12688.
[29] C. Tong, S. Zhang, T. Zhong, Z. Fang, H. Liu, Highly fibrillated and intrinsically flame-retardant nanofibrillated cellulose for transparent mineral filler-free fire-protective coatings, Chem. Eng. J. 419 (2021) 129440, https://doi.org/10.1016/j.cej.2021.129440.
[30] J. Peng, S. Xie, T. Liu, D. Wang, R. Ou, C. Guo, Q. Wang, Z. Liu, High-performance epoxy vitrimer with superior self-healing, shape-memory, flame retardancy, and antibacterial properties based on multifunctional curing agent, Compos. Part B 242 (2022) 110109, https://doi.org/10.1016/j.compositesb.2022.110109.
[31] C. Hu, J. Li, X. Pan, Y. Zeng, Intrinsically flame-retardant vanillin-based PU networks with self-healing and reprocessing performances, Ind. Crops Prod. 200 (5) (2023) 116828, https://doi.org/10.1016/j.indcrop.2023.116828.
[32] X. Wang, S. Zhan, Z. Lu, J. Li, X. Yang, Y. Qiao, Y. Men, J. Sun, Healable, recyclable, and mechanically tough polyurethane elastomers with exceptional damage tolerance, Adv. Mater. 32 (50) (2020) e2005759, https://doi.org/10.1002/adma.202005759.
[33] P. Hu, W. Chen, Y. Wang, T. Chen, X. Qian, W. Li, J. Chen, J. Fu, Fatigue-free and skin-like supramolecular ion-conductive elastomeric interphases for stable lithium metal batteries, ACS Nano 17 (16) (2023) 16239–16251, https://doi.org/10.1021/acsnano.3c06171.
[34] H. Wang, J. Xu, X. Du, Z. Du, X. Cheng, H. Wang, A self-healing polyurethane-based composite coating with high strength and anti-corrosion properties for metal protection, Compos. Part B 225 (2021) 109273, https://doi.org/10.1016/j.compositesb.2021.109273.
[35] H. Tan, L. Zhang, X. Ma, L. Sun, D. Yu, Z. You, Adaptable covalently cross-linked fibers, Nat. Commun. 14 (1) (2023) 2218, https://doi.org/10.1038/s41467-023-37850-w.
[36] B. Zheng, T. Liu, J. Liu, Y. Cui, R. Ou, C. Guo, Z. Liu, Q. Wang, Spider silk-inspired dynamic covalent polyurethane with fast repairing, shape memory, and strong dynamic adhesion via lignin enhanced microphase separation, Compos. Part B 257 (2023) 110697, https://doi.org/10.1016/j.compositesb.2023.110697.
[37] L. Chen, D. Zhao, X.L. Wang, Y.Z. Wang, Durable macromolecular firefighting for unsaturated polyester via integrating synergistic charring and hydrogen bond, Chem. Eng. J. 443 (1) (2022) 136365, https://doi.org/10.1016/j.cej.2022.136365.
[38] Y. Fang, X. Du, S. Yang, H. Wang, X. Cheng, Z. Du, Sustainable and tough polyurethane films with self-healability and flame retardance enabled by reversible chemistry and cyclotriphosphazene, Polym. Chem. 10 (30) (2019) 4142–4153, https://doi.org/10.1039/c9py00680j.
[39] X. Ye, C. Zhan, B. Wang, T. Sai, C. Zhang, J. Li, Z. Guo, S. Huo, Engineering sulfonated carbon black for flame-retardant and smoke-suppressive polycarbonate with well-preserved mechanical performances, Polym. Degrad. Stab. 230 (2024) 111012, https://doi.org/10.1016/j.polymdegradstab.2024.111012.
[40] Y. Xue, M. Zhang, S. Huo, Z. Ma, M. Lynch, B.T. Tuten, Z. Sun, W. Zheng, Y. Zhou, P. Song, Engineered functional segments enabled mechanically robust, intrinsically fire-retardant, switchable, degradable polyurethane adhesives, Adv. Funct. Mater. (2024) 2409139, https://doi.org/10.1002/adfm.202409139.
[41] J.R. Xavier, S.P. Vinodhini, Advanced nanocomposite coating for aluminium alloy with enhanced corrosion resistance, flame retardancy, and mechanical strength in aircraft manufacturing industries, Colloids Surf., A 698 (2024) 134543, https://doi.org/10.1016/j.colsurfa.2024.134543.
[42] J.R. Xavier, Multilayered nanocomposite coatings for enhanced anticorrosive, flame retardant, and mechanical properties in automobile and aerospace industries, J. Appl. Polym. Sci. 140 (24) (2023) 53943, https://doi.org/10.1002/app.53943.
[43] J.R. Xavier, S.P. Vinodhini, Improved anticorrosion, flame retardant and mechanical behaviors of multifunctional polyurethane nanocomposite coatings for industrial applications, Polym. Degrad. Stab. 213 (2023) 110370, https://doi.org/10.1016/j.polymdegradstab.2023.110370.
[44] S. Wang, S. Lou, P. Fan, L. Ma, J. Liu, T. Tang, A novel aromatic imine-containing DOPO-based reactive flame retardant towards enhanced flame-retardant and mechanical properties of epoxy resin, Polym. Degrad. Stab. 213 (2023) 110364, https://doi.org/10.1016/j.polymdegradstab.2023.110364.
[45] S. Yang, S. Wang, X. Du, Z. Du, X. Cheng, H. Wang, Mechanically robust self-healing and recyclable flame-retarded polyurethane elastomer based on thermoreversible crosslinking network and multiple hydrogen bonds, Chem. Eng. J. 391 (2020) 123544, https://doi.org/10.1016/j.cej.2019.123544.
[46] J.R. Xavier, R. Bhaskar, S. Subramanian, Multifunctional graphitic carbon nitride/manganese dioxide/epoxy nanocomposite coating on steel for enhanced anticorrosion, flame retardant, mechanical, and hydrophobic properties, J. Ind. Eng. Chem. 134 (2024) 514–536, https://doi.org/10.1016/j.jiec.2024.01.015.
[47] H. Tong, Y. Chen, Y. Weng, S. Zhang, Biodegradable-renewable vitrimer fabrication by epoxidized natural rubber and oxidized starch with robust ductility and elastic recovery, ACS Sustain. Chem. Eng. 10 (24) (2022) 7942–7953, https://doi.org/10.1021/acssuschemeng.2c01163.
[48] B. Zhang, X. Yang, X. Lin, H. Shang, Q. Liu, H. Wang, S. Liu, X. Xu, F. Dong, High-strength, self-healing, recyclable, and catalyst-free bio-based non-isocyanate polyurethane, ACS Sustain. Chem. Eng. 11 (15) (2023) 6100–6113, https://doi.org/10.1021/acssuschemeng.3c01181.
[49] L.J. Hamernik, W. Guzman, J.S. Wiggins, Solvent-free preparation of imine vitrimers: leveraging benzoxazine crosslinking for melt processability and tunable mechanical performance, J. Mater. Chem. A 11 (38) (2023) 20568–20582, https://doi.org/10.1039/d3ta04351g.
[50] H. Fang, F. Zhang, Y. Zhao, X. Gao, W. Zhou, G. Qi, Y. Ding, H.H. Winter, Rheology of smectic liquid crystalline elastomers with dynamic covalent bonds, Macromolecules 56 (19) (2023) 7808–7817, https://doi.org/10.1021/acs.macromol.3c00887.
[51] X. Ma, X. Wang, H. Zhao, X. Xu, M. Cui, N.E. Stott, P. Chen, J. Zhu, N. Yan, J. Chen, High-performance, light-stimulation healable, and closed-loop recyclable lignin-based covalent adaptable networks, Small 19 (40) (2023) 2303215, https://doi.org/10.1002/smll.202303215.
[52] C. Huyan, D. Liu, C. Pan, D. Wang, Z. Guo, X. Zhang, S. Dai, B. Bin Xu, F. Chen, Thermally recyclable and reprocessable glass fiber reinforced high performance thermosetting polyurethane vitrimer composites, Chem. Eng. J. 471 (1) (2023) 144478, https://doi.org/10.1016/j.cej.2023.144478.
[53] C. Tretbar, J. Castro, K. Yokoyama, Z. Guan, Fluoride-catalyzed siloxane exchange as a robust dynamic chemistry for high-performance vitrimers, Adv. Mater. 35 (28) (2023) 2303280, https://doi.org/10.1002/adma.202303280.
[54] D.M. Xie, Y.X. Zhang, Y.D. Li, Y. Weng, J.B. Zeng, Castor oil-derived sustainable poly(urethane urea) covalent adaptable networks with tunable mechanical properties and multiple recyclability based on reversible piperidine-urea bond, Chem. Eng. J. 446 (15) (2022) 137071, https://doi.org/10.1016/j.cej.2022.137071.
[55] P. Li, X. Zhang, Q. Yang, P. Gong, C.B. Park, G. Li, Sustainable polyester vitrimer capable of fast self-healing and multiple shape-programming via efficient synthesis and configuration processing, J. Mater. Chem. A 11 (20) (2023) 10912–10926, https://doi.org/10.1039/d3ta00302g.
[56] X. Wang, J. Xu, Y. Zhang, T. Wang, Q. Wang, S. Li, Z. Yang, X. Zhang, A stretchable, mechanically robust polymer exhibiting shape-memory-assisted self-healing and clustering-triggered emission, Nat. Commun. 14 (1) (2023) 4712, https://doi.org/10.1038/s41467-023-40340-8.
[57] J. Zhang, Z. Yin, L. Ren, Q. Liu, L. Ren, X. Yang, X. Zhou, Advances in 4D printed shape memory polymers: from 3D printing, smart excitation, and response to applications, Adv. Mater. Technol. 7 (9) (2022) 2101568, https://doi.org/10.1002/admt.202101568.